J. Fluid Mech. (1981), *vol.* 102, *pp.* 221–248
Printed in Great Britain

Layered double-diffusive convection in porous media

By R. W. GRIFFITHS
Department of Applied Mathematics and Theoretical Physics, University of Cambridge

(Received 12 February 1979 and in revised form 24 November 1979)

In this paper it is shown that layered double-diffusive convection of a fluid within a porous medium is possible. A thin 'diffusive' interface was observed in a Hele Shaw cell and in a laboratory porous medium, with salt and sugar or heat and salt as the diffusing components. Heat–salt and salt–sugar fluxes through two-layer convection systems were measured and are compared with predictions of a model. For the thermohaline system the salt and heat buoyancy fluxes are approximately in the ratio $r \simeq \epsilon \tau_m^{\frac{1}{2}}$, where ϵ is the porosity and τ_m is the appropriate ratio of diffusivities. The behaviour of the heat flux is explained in terms of a coupling between purely thermal convection within each convecting layer and diffusion through the density interface. Salinity gradients are important only within the interface. The presence of a 'diffusive' interface in the Wairakei geothermal system is postulated. The ratio of heat and salt fluxes (that can be estimated from existing observations) through this convection system is consistent with the laboratory flux ratio.

1. Introduction

Convection of a viscous fluid can be driven by the differential diffusion of two properties such as heat and salt when the properties contribute opposing vertical density gradients (Turner 1973). In the laboratory the resulting convection is often characterized by a number of well-mixed convecting layers, each of limited vertical extent and separated from each other by relatively thin density steps. When the lower layer is warmer and more saline than the upper layer, transport of salt and heat through the 'diffusive' interfaces is by molecular diffusion (apart from some turbulent entrainment). The more rapid diffusion of heat provides a net buoyancy flux to drive the convection. In laboratory experiments (Turner 1965; Crapper 1975; Marmorino & Caldwell 1976) the buoyancy fluxes due to salt and heat are in the ratio $0{\cdot}15 \pm 0{\cdot}02$ so long as the heat flux is not too small. Griffiths (1979) also found that several solutes mix through such a heat–salt interface at rates that depend strongly upon the individual molecular diffusion coefficients. In the inverted system (warm, saline water over cooler, fresher water with the lower layer again more dense) a thin 'salt finger' interface develops (Turner 1967). This density interface allows efficient vertical transport of the property with smaller molecular diffusivity.

In order to understand the fluxes through the 'diffusive' interface in a viscous fluid, a model for the interface has been constructed by Linden & Shirtcliffe (1978). They considered the boundary-layer flow of high-Rayleigh-number thermal convection in the mixed layers. At Rayleigh numbers greater than 10^5 (Foster 1971) this convection involves the intermittent growth by molecular diffusion of thin buoyant boundary

0022-1120/81/4632-2850 $02.00

layers, with the subsequent release of buoyant elements into the convecting layer. The boundary layer grows until a local Rayleigh number based upon the boundary-layer thickness exceeds a critical value (of order 10^3) and, after this time, all of the buoyant fluid takes part in convection in the form of thin, two-dimensional plumes. This type of convection, modified little by the presence of two components, was assumed to provide the boundary conditions for the 'diffusive' interface.

In the models for double-diffusive interfaces in a viscous fluid it has also been assumed that inertial fluid motions are not necessary in order to maintain thin density interfaces against spreading by diffusion or salt finger convection. Because the vertical density profile through the interface can be discontinuous only if inertial forces are present, this assumption is implicit in a boundary condition which states that the density profile is always continuous across the interface edges. This is equivalent to saying that all of the buoyant fluid and only the buoyant fluid in the boundary layer takes part in convection. On the other hand, such interfaces are observed to migrate (Marmorino & Caldwell 1976; Schmitt 1979). This implies a net flux of fluid through the interface and suggests that nonbuoyant fluid is entrained from the density gradient. At larger interfacial Froude numbers, the convection of the mixed layers is seen to penetrate the density gradient of the interface and excite interfacial waves.

Another case of double-diffusive convection – that of layered thermohaline convection within a porous medium – is studied in this paper. Such convection has not previously been considered but might occur, in the 'diffusive' sense, within geothermal systems if hot brines remain beneath cooler and less saline groundwaters. Both heat and salt fluxes could then be significantly different from those given by thermal convection throughout the whole depth of the fluid and two different chemical environments could be maintained. The study of double-diffusive interfaces in a porous medium can also add further understanding to the viscous fluid phenomena already mentioned. For the buoyancy-driven convection of a fluid within a porous material, inertial forces are negligible. The possibility of entrainment of non-buoyant fluid from a density gradient into a convecting region is therefore reduced. Flow geometries produced by layered convection will also differ from those in visous fluid convection as there can be no advection or diffusion of vorticity. On the other hand, thermal convection again takes the form of a boundary-layer flow; in this case at only moderately supercritical values of the appropriate Rayleigh number.

Current understanding of purely thermal convection is outlined in § 2. The results will be required in subsequent sections in order to help describe the fluxes through a two-layer system. Qualitative laboratory observations in a Hele Shaw cell analogue to a porous medium are presented in § 3 and indicate that a thin 'diffusive' interface can continue to exist on the laboratory time scale. These experiments use salt and sugar as the two diffusing components, and show that convection maintains the thin density interface against spreading by diffusion. We consider in this paper only the case in which potential energy for convection is supplied by the property with the greater diffusivity, although a linearized stability analysis (Nield 1968) predicts that salt fingers within a porous medium are also possible.† Some preliminary theoretical ideas about the fluxes through a 'diffusive' interface in a heat–solute system are given

† Porous medium salt fingers cannot easily be studied in the laboratory, where their horizontal length scale is comparable to the grain size of the material. Fingers obeying the viscous fluid equations will then form instead.

in § 4. These ideas are not intended to be absolute predictions but are to be compared (in § 7) with the results of experiments using a porous medium of glass spheres and heat and salt as the diffusing components. The experiments and measured fluxes are described in § 5 and § 6. Finally the presence of a 'diffusive' density interface in a real geothermal system is considered in § 8.

2. Thermal convection

For a horizontal layer of saturated porous material of depth H, heated uniformly from below, suitable units of length, temperature, pressure, time and velocity are H, ΔT, $\rho_0 \nu \kappa_m / k$, H^2/κ_m and κ_m/H respectively, where ρ_0 is a mean fluid density, ν is the kinematic viscosity and k is the permeability. The temperature difference between boundaries is ΔT and the thermal diffusivity is $\kappa_m = K_m/(\rho c)_f$, where K_m is the thermal conductivity of the saturated medium and $(\rho c)_f$ is the volumetric heat capacity of the fluid. Two parameters which describe the flow are the Rayleigh number,

$$R_m = g\alpha \Delta T k H / \kappa_m \nu,$$

and the Prandtl–Darcy number $B = (\nu/\kappa_m)(H^2/k)$, where α is the coefficient of thermal expansion. A factor B^{-1} multiplies the inertia terms of the momentum equation (see Wooding 1957) and we will only consider the limit $B \to \infty$ that holds for an ideal porous medium.

Theoretical and experimental investigations of the heat flux at slightly supercritical Rayleigh numbers ($40 < R_m < 200$) have given an approximately linear relationship between the Nusselt number, Nu, and the Rayleigh number (e.g. Elder 1967). The heat flux is then independent of the layer depth. For larger values, $R_m > 200$, empirical heat fluxes begin to fall below those predicted by this linear relation. In order to explain the observed behaviour, several authors have considered the development of a boundary-layer flow at higher Rayleigh numbers. These models and the existing experimental results are reviewed by Booker & Hartline (1981). They conclude from a boundary-layer scale analysis that

$$Nu \approx R_m^{\frac{1}{2}} \tag{1}$$

is the appropriate asymptotic form for large R_m and that equation (1) also describes the existing heat-flux measurements at $R_m > 10^3$. At intermediate values of the Rayleigh number there is a gradual transition from the behaviour at small Rayleigh numbers to that at high Rayleigh numbers. In this range ($100 < R_m < 1000$) we find that the simple relation

$$Nu = 1{\cdot}55(R_m/40)^{\frac{1}{2}} \tag{2}$$

provides a reasonable fit to the experimental data. Although this form cannot give an accurate prediction of the heat-flux behaviour, such a simple form will be useful in § 6, where it will be seen that the present experiments have thermal Rayleigh numbers in the range $200 < R_m < 2000$. It will also be seen that the thermal boundary-layer thickness in our experiments is larger than the individual grain size, so that the medium can be considered to have infinitesimal grains when discussing the heat transport (see Booker & Hartline). Note that (2) was obtained by Robinson & O'Sullivan (1976) by fitting a boundary-layer scale analysis (different from that of Booker & Hartline) to the results of a series of numerical experiments over the range $100 < R_m < 3000$.

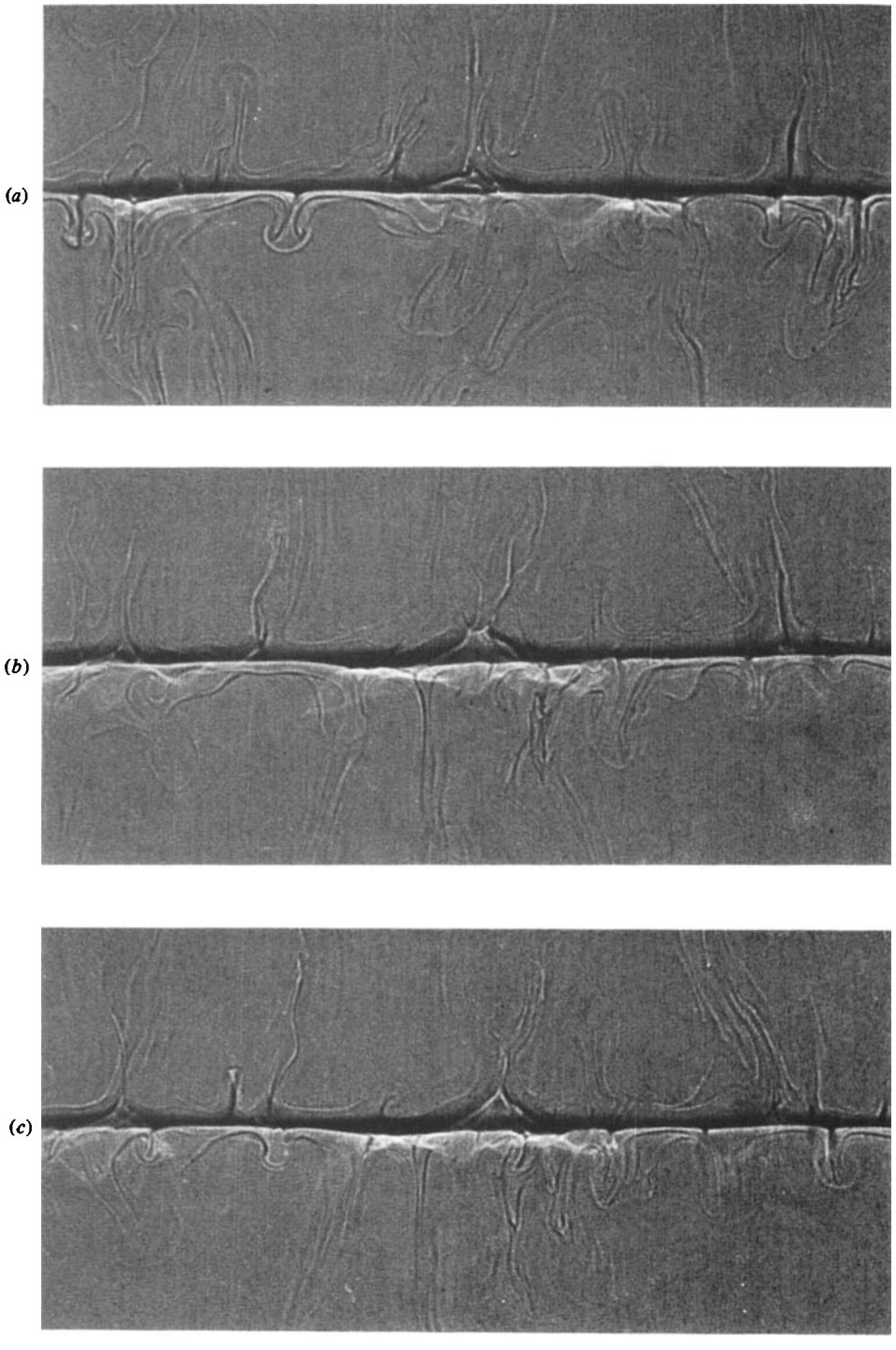

FIGURE 1. Shadowgraph photographs of a two-solute interface in a Hele Shaw cell. Frames are at about 1 min intervals and $\alpha\Delta S/\alpha\Delta T \sim 1{\cdot}2$.

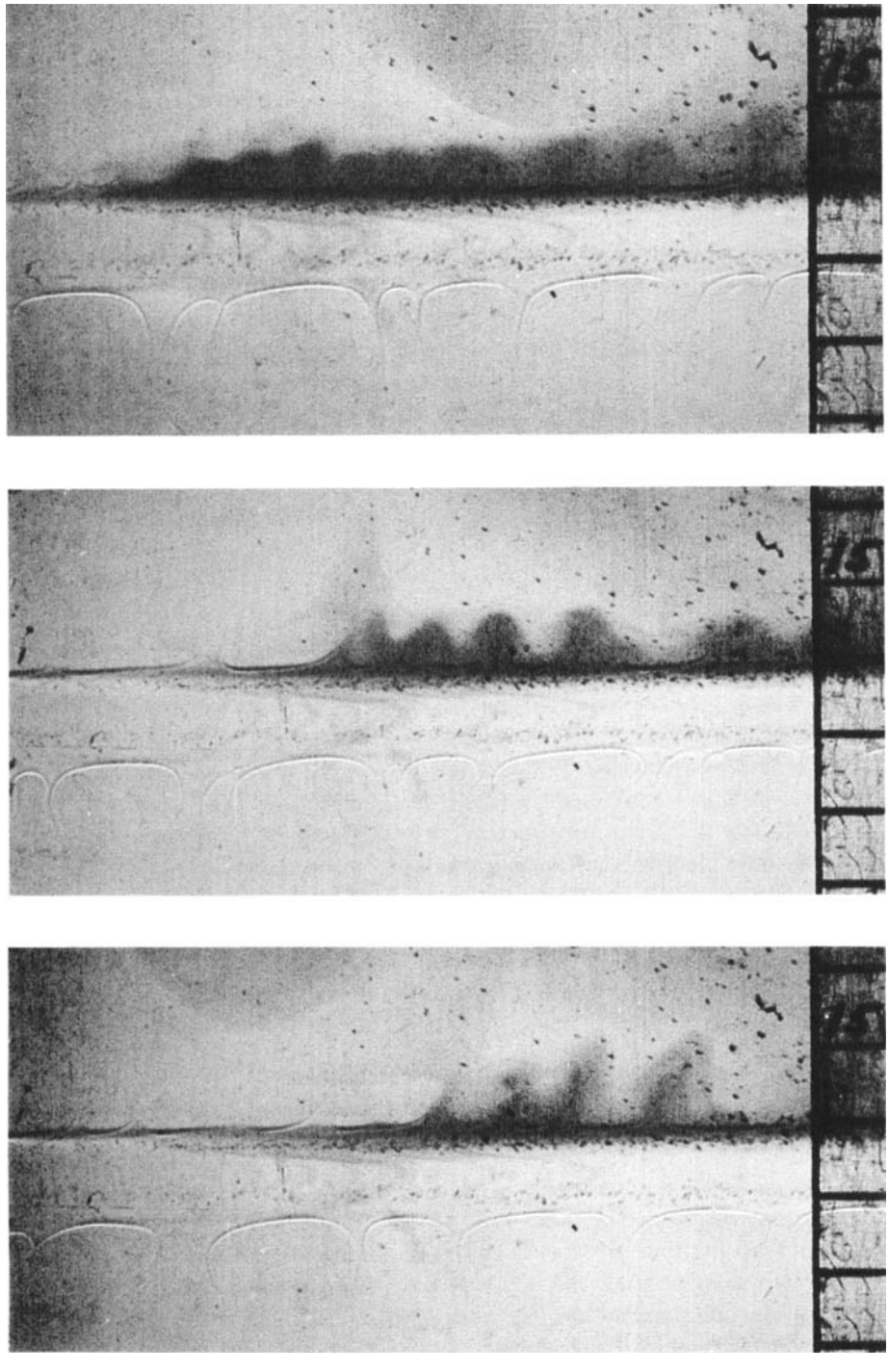

FIGURE 2. Shadowgraphs of the interface of figure 1 after the system has run down for 24 hours. Scale is in centimetres. Some dye was placed in the top layer and collected on the interface just before this sequence. Frames are at about 30 s intervals.

3. Observations in a Hele Shaw cell

Convection within a porous medium can be modelled, and more easily visualized, in a Hele Shaw cell. The analogy between the two will be valid if the velocity, U, and the smallest length scale of the motion, δ, satisfy the conditions $b/\delta \ll 1$, $Ub^2/\nu\delta \ll 1$ and $Ub^2/\kappa\delta \ll 1$, where b is the distance between the cell walls (Wooding 1960).

An isothermal, two-layer convection system was established in a Hele Shaw cell by placing a layer of sodium chloride (T) solution (with a concentration of $T = 133‰$, or grams of solute per kilogram of solution) onto a layer of sucrose (S) solution ($S = 246‰$). This gave an initial ratio of component density steps of $\beta\Delta S/\alpha\Delta T \simeq 1{\cdot}15$. The salt has a molecular diffusivity approximately three times that of sugar. Each layer was 13 cm deep, with $b \simeq 0{\cdot}1$ cm. In figures 1 and 2 are shown shadowgraph photographs taken at several times during an 8-day period as the system ran-down to higher density ratios, For individual mushroom-shaped plumes, $U \sim 10^{-2}\,\mathrm{cm\,s^{-1}}$ and $\delta \sim 0{\cdot}5$ cm. Hence $b/\delta \sim 0{\cdot}2$, $Ub^2/\nu\delta \sim 0{\cdot}02$ and $Ub^2/\kappa\delta \sim 20$, where the diffusivity of both solutes is of the order of $10^{-5}\,\mathrm{cm^2\,s^{-1}}$. Thus the Hele Shaw model tends to break down due to the small solute diffusivity, although the momentum diffuses rapidly across the space occupied by the fluid.

The sequence of figure 1 shows highly unsteady motion, with plumes intermittently appearing and breaking away from the interface edge. In figure 2 the system has run down to a higher density ratio and only plumes such as those still visible below the interface existed before a small amount of dye was injected into the top layer. These plumes move slowly along the interface. After the dyed fluid spreads out on the interface there is first a period in which diffusion is important, then disturbances with a small length scale determined by some local criterion are amplified. The dye in the shadowgraph of figure 2(a) shows only slowly growing, roughly sinusoidal, motions with a length scale of 0·5 cm. As seen in figures 2(b) and (c), more rapid motions follow and the horizontal length scale of the vertical plumes increases. As in the viscous fluid case the fluxes of salt and sugar are determined by the coupling between this form of convection and the diffusion through the interface. The flow adjacent to the interface is also very similar to that predicted and observed at the thermal boundary layer on a heated flat plate (Elder 1968; Robinson 1976).

4. Theoretical arguments

Dimensional reasoning indicates those parameters of a two-layer system that may influence the heat and salt fluxes through the 'diffusive' interface in a porous medium. There are the individual contributions ($\alpha\Delta T$ and $\beta\Delta S$) of temperature and salinity to the total density difference ($\Delta\rho$) between layers and there are the macroscopic molecular diffusivities (κ_m and D) that apply to the diffusion of heat and solute through distances much greater than the scale of individual pores. The fluxes may also be dependent upon the parameters (R_m and B) of the layer convection and upon the porosity, ϵ, of the medium. The dimensionless interfacial heat flux may be expressed as

$$Nu = g(R_\rho, R_m, B, \tau_m, \epsilon), \tag{3}$$

where Nu is a Nusselt number, $R_\rho = \beta\Delta S/\alpha\Delta T$ and $\tau_m = D/\kappa_m$ is the ratio of molecular diffusivities appropriate to the saturated medium.

Only the limit $B \to \infty$ will be considered. As in the viscous fluid case (Turner 1965) a dimensionless heat flux may be defined by comparing the interfacial flux, F_T, with the heat flux, F^P, that would flow if the interface was replaced by a thin, conducting and impermeable solid plane. Then the following postulate leads to a simplification of (3) that will later be tested experimentally: for given porosity and molecular diffusivities, the nature of the interface and the transport of salt alter the heat-transporting properties of the convection *in each layer* only by altering the temperature boundary conditions for that layer. An equivalent statement is that salinity gradients are important only within the interface and that the interface behaves as a rigid boundary. According to (2) this postulate implies that the flux through each convecting layer behaves as $F_T \propto H^{-\frac{1}{3}}$. If the system is in a steady state, F_T is the flux through the interface. Since (2) also gives the 'solid plane' flux, F^P, the dimensionless heat flux is independent of layer depth and must take the form

$$F_T^* \equiv \frac{F_T}{F^P} = f(R_\rho, \tau_m, \epsilon). \tag{4}$$

With fixed molecular properties and a given porous material the dimensionless heat flux varies only with the density ratio, R_ρ.

The ratio of buoyancy (density) fluxes

$$r \equiv \beta F_S / \alpha F_T \tag{5}$$

should be a function of those parameters included in (3). We also know that the buoyancy flux βF_S due to solute is carried through the mixed layers by the thermally driven convection. However, there is no justification for us to assume that F_S and F_T will take the same dependence upon the thermal Rayleigh number (or the depth scale H). Therefore, a dependence of the flux ratio, r, upon the Rayleigh number, R_m, cannot be dismissed.

On the other hand, it is possible to estimate both the ratio of buoyancy fluxes and the dimensionless heat flux by considering the boundary-layer flow at the interface edge. If we assume that the porous medium convection is of the highly unsteady form visible in figure 1, then a direct analogy can be drawn with the 'diffusive' interface in a viscous fluid. In both cases the interface is bounded by intermittent, high-Rayleigh-number convection. As in the model of Linden & Shirtcliffe (1978), we will describe the interface itself in terms of a central region through which all transport is by molecular diffusion and outer regions which couple the diffusion to the convection. The latter region is not understood for the real porous medium case. This is because the boundary-layer flows in the heat–salt experiments (reported in § 5) form a cellular, though still unsteady, structure. There are then horizontal property variations at the interface edges and horizontal flow in the boundary layers. In the absence of a simple model to describe the influence of slowly varying spatial inhomogeneities upon the interfacial fluxes, we will consider only temporal variations of T, S and ρ.

In order to find an estimate of the flux ratio, we use the condition that the vertical density gradient is continuous throughout the interface. That is, all of the buoyant fluid in the boundary layer and only this buoyant fluid takes part in convection. This requires equal and opposite density steps due to T and S at the interface edges. Idealized profiles of αT, βS and ρ immediately after buoyant elements have been ejected from the boundary layers are sketched in figure 3. There are steps $\frac{1}{2}\alpha\delta T$ and

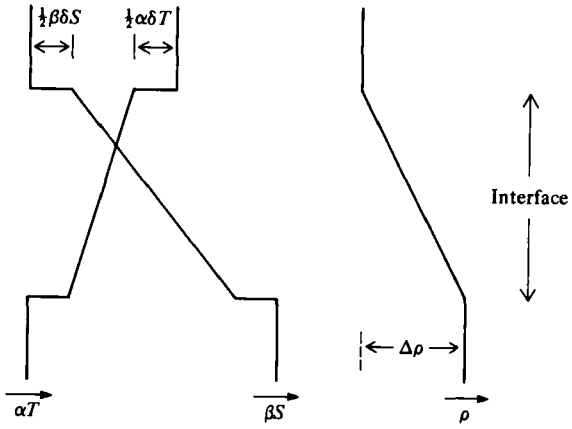

FIGURE 3. Idealized profiles of αT, βS and density, ρ, through a 'diffusive' interface with intermittent boundary layers just before a buoyant boundary layer begins to grow. The property with the greatest diffusivity provides the potential energy for convection. In this diagram, $\Delta\rho$ is the density difference between layers.

$\frac{1}{2}\beta\delta S$ at the interface edges. The existence of such steps (or at least steep gradients) in the Hele-Shaw flow of figures 1 and 2 is indicated by the sharp refractive index changes. New boundary layers are created by vertical molecular diffusion from the sharp steps of figure 3. The flux ratio is determined by the ratio of T and S anomalies in the diffusive boundary layer when it breaks away. Steps of equal magnitude ($\beta\delta S = \alpha\delta T$) now imply that the flux ratio is independent of the overall concentration differences between layers provided that $h \gg 4(\kappa_T t_*)^{\frac{1}{2}}$, where h is the interface thickness and t_* a time scale for the intermittent convection (Linden & Shirtcliffe). For two solutes, integration of the error function diffusion profiles outside the interface edge yields $r \simeq \tau^{\frac{1}{2}}$, where $\tau = \kappa_S/\kappa_T$ is the ratio of diffusivities in the fluid. This result, and the arguments leading to it, are identical with those of the viscous fluid case.

The ratio of salt and heat fluxes through an interface in a porous medium is influenced by two additional factors. First, a macroscopic diffusion coefficient D for solute must be defined to include the tortuosity $\mathscr{T}$ of paths through the fluid within the medium (see De Wiest 1969). For a homogeneous, isotropic medium we can write $D = \mathscr{T}\kappa_S$, where κ_S is the solute diffusivity in the fluid. Experiments with beds of glass beads have given $\mathscr{T} \simeq \frac{2}{3}$ (see Saffman 1960). As before, the ratio of diffusivities for solute and heat is $\tau_m = D/\kappa_m$.

Second, heat travels through both solid and liquid while the solute is confined to a fraction ϵ of the total volume. The coefficient D describes the macroscopic rate of diffusion of solute through a saturated medium. Hence the solute buoyancy anomaly in the diffusive boundary layer is given by $\epsilon \int_{z_1}^{\infty} \beta S(z,t)\,dz$, where z is the vertical coordinate and $z = z_1$ at the (upper) edge of the interface. The buoyancy fluxes of solute and heat through the intermittent boundary layer are in the ratio

$$r = \epsilon \int_{z_1}^{\infty} \beta S(z,t)\,dz \Big/ \int_{z_1}^{\infty} \alpha T(z,t)\,dz.$$

This becomes (see Linden & Shirtcliffe)

$$r \simeq \epsilon \tau_m^{\frac{1}{2}}. \tag{6}$$

This flux ratio is a constant, independent of R_ρ and R_m, for a given medium and fixed molecular properties.

To continue the model for the 'diffusive' interface, the ratio (6) may be equated to the ratio of diffusive buoyancy fluxes down T and S gradients through the interface centre. Provided that $h \gg 4(\kappa_T t_*)^{\frac{1}{2}}$, these gradients are steady and close to linear. Then

$$r \simeq \frac{\epsilon D}{\kappa_m}\left(\frac{\beta\Delta S - \beta\delta S}{\alpha\Delta T - \alpha\delta T}\right). \tag{7}$$

From (7) and the condition $\beta\delta S = \alpha\delta T$, the temperature step at the interface edge becomes

$$\frac{\delta T}{\Delta T} \simeq \frac{1-(\epsilon\tau_m/r)R_\rho}{1-\epsilon\tau_m/r}. \tag{8}$$

Equation (8) has been written in terms of r, which may be found empirically or from (6), to facilitate comparison with experiments.

The flux of heat through the interface can now be estimated. Note that the total effective temperature drop across each convecting layer must be equal to the (idealized) temperature step, $\frac{1}{2}\delta T$, at the interface edge. The fluid that replaces ejected buoyant fluid at the upper interface edge (shown by the profiles of figure 3) is the coldest fluid in the upper convecting layer. This fluid is then heated through an amount $\frac{1}{2}\delta T$ before joining an upward-moving plume. In the cellular motions at only moderate Rayleigh numbers (discussed in §§ 6 and 7) $\frac{1}{2}\delta T$ becomes the horizontal temperature difference between plumes. However, it is not clear how the model predictions are influenced by the observed horizontal property variations.

The transport equation (2) is again assumed to describe the heat flux through purely thermal convection. Then our earlier hypothesis (which stated that salinity gradients are only important within the interface and that the edge of the interface behaves as a rigid boundary) can be used to express the thermal buoyancy fluxes in the form $\alpha F_T = (gk/\nu)^{\frac{3}{2}}(\kappa_m/H)^{\frac{1}{2}}(\frac{1}{2}\alpha\delta T)^{\frac{5}{2}}$ and $\alpha F^P = (gk/\nu)^{\frac{3}{2}}(\kappa_m/H)^{\frac{1}{2}}(\alpha\Delta T)^{\frac{5}{2}}$. The dimensionless heat flux becomes $F_T^* = (\delta T/2\Delta T)^{\frac{5}{2}}$ or, using (8),

$$F_T^* \simeq \left[\frac{1}{2}\left(\frac{1-(\epsilon\tau_m/r)R_\rho}{1-\epsilon\tau_m/r}\right)\right]^{\frac{5}{2}}. \tag{9}$$

The above discussion indicates that the role of four parameters must be studied in a complete experimental investigation of the 'diffusive' interface in a porous medium. The experiments described in § 5 are a study of the set R_ρ, R_m and τ_m only, but the porosity ϵ is only expected to be important in the manner of (6). Relations (6), (8) and (9) will be compared with measured fluxes and temperatures in § 7.

5. Laboratory experiments

Apparatus

Measurements were taken of fluxes through a 'diffusive' interface within a porous medium of roughly uniform glass spheres. The pore space was filled with two layers of aqueous sodium chloride solution. Two different boxes were used to contain the saturated medium and a comparison of the heat flux measurements from the two boxes

reduced the possibility of unknown systematic errors. Both boxes had Perspex walls (1 cm thick) but could be heated from below and cooled from above. Box A was 30 cm deep with a horizontal area of 20 cm × 10·6 cm. Heat was supplied to its metal base from a hot plate to which the power supply could be controlled. The saturated medium was cooled by circulating water from a constant-temperature bath through a metal lid. Box B was a cube of 20 cm side with constant-temperature water baths providing both heating and cooling. The bath temperatures were controlled to $\pm 0{\cdot}02\,^{\circ}\mathrm{C}$ while the water circulated (at $\sim 50\,\mathrm{cm^3\,s^{-1}}$) through a maze of channels in the aluminium base and lid to supply vertical heat fluxes of up to $10\,\mathrm{cal\,s^{-1}}$. Both boxes had, in the centre of a tapered lid, a small hole which led up to a tube of larger diameter. This tube served as a reservoir of fluid for the upper layer, allowing the lid to remain in contact with the fluid despite the withdrawal of samples during an experiment.

Heat-flux meters (HFM) were included in both the base and lid of box B but only in the base of box A. Each HFM consisted of a sheet of polypropylene 0·1 cm thick separating a heated (or cooled) aluminium block from an inner Al plate (0·8 cm thick). The inner plate was in contact with the contents of the box. Thermistors attached to the Al on each side of the insulating layer enabled the temperature difference to be found with an uncertainty of 0·02 °C. Side-wall heat transfer was reduced to $(3{\cdot}4 \pm 0{\cdot}2) \times 10^{-5}\,\mathrm{cal\,cm^{-2}\,s^{-1}\,^{\circ}C^{-1}}$ for box A and $(1{\cdot}8 \pm 0{\cdot}1) \times 10^{-5}\,\mathrm{cal\,cm^{-2}\,s^{-1}\,^{\circ}C^{-1}}$ for box B by placing polystyrene foam on all surfaces.

Each HFM was calibrated individually by filling the box with a known volume of distilled water, insulating all boundaries and then heating (or cooling) through the HFM while the water was stirred. The heat transfer coefficient, $\Gamma\,(\mathrm{cal\,s^{-1}\,^{\circ}C^{-1}})$, was then obtained by equating the time-integrated flux through the thermal 'resistor' to the sum of the heat gained by the water and the heat lost from the system. The period required for calibration was sufficiently short to keep the integrated side-wall losses to less than 2 % of the heat gained by the water. Results were corrected to account for the heat capacity of the Perspex walls and Al plate. Uncertainties in Γ are thought to be less than 3 %.

Resistance thermometers were embedded in the beads in order to obtain average temperatures for horizontal planes near the centre of each layer. Horizontal averages were necessary due to the large spatial temperature variations within a convecting layer. Each thermometer consisted of 6 m of fine insulated wire which crossed the width of the box at a regular spacing. The unbalanced voltage from a bridge circuit for each thermometer was displayed on a chart recorder and thermometers were calibrated before and after each experiment. A bridge supply voltage was chosen so that each thermometer dissipated only $4 \times 10^{-4}\,\mathrm{cal\,s^{-1}}$, or 0·02 % of the smallest heat flux measured. At the same time, vertical temperature profiles through the fluid density interface were obtained by embedding a vertical array of six glass-bead thermistors near the centre of the box. These thermistors were fixed $1{\cdot}5 \pm 0{\cdot}1$ cm from each other and the resistance of each was calibrated to within an uncertainty of $\pm 0{\cdot}02\,^{\circ}\mathrm{C}$.

Withdrawal of fluid samples and injection of dye were achieved by mounting syringe needles in one wall of each box. However, a number of trial samples taken from different points in the medium led to a large scatter in measured salinities. Consequently, the horizontal variations within each layer were averaged by withdrawing fluid through six small tubes until a (mixed) volume of 1 ml was reached. The density

of samples was measured to within an uncertainty of less than 2×10^{-5} g cm^{-3} at $25{\cdot}00 \pm 0{\cdot}01$ °C with a digital precision density meter (model DMA 02C, Anton Paar K.G., Austria). The sodium chloride concentration, S (in grams of solute per gram of solution) is then given by polynomials of Ruddick & Shirtcliffe (1979).

A two-layer system in which the property (S) with smaller diffusivity was sucrose and the property (T) with the greater diffusivity was salt was also studied in order to test the dependence of the flux ratio upon the ratio of diffusivities. A medium of 0·3 cm diameter glass beads was used in box B. Two layers of equal depth (10 cm) were established, initially with $\Delta T = 126\,‰$ and $\Delta S = 247\,‰$, and the system allowed to run down. In this case both the density and conductivity of small samples were measured. The dimensionless sugar concentration, S, and salt concentration, T, were again given by the data of Ruddick & Shirtcliffe, this time by inverting their density and conductivity polynomials, $\rho(T, S)$ and $\lambda(T, S)$ respectively.

The porous media

Two bead diameters, $l = 0{\cdot}3$ cm and $l = 0{\cdot}6$ cm, were used for the thermohaline experiments. These, and changes of ΔT, allowed variations of the thermal Rayleigh number for the convection. Both sizes gave a porosity $\epsilon = 0{\cdot}38$, reproducible to within $\pm 0{\cdot}01$. The measured thermal diffusivity was $\kappa_m = 2{\cdot}6 \times 10^{-3}$ cm^2 s^{-1}, a value that is roughly twice that of the fluid alone and is considered to have an uncertainty of 10 %. The measured permeabilities are $k \approx 9{\cdot}4 \times 10^{-5}$ cm^2 for a medium of 0·3 cm beads and $k \approx 3{\cdot}1 \times 10^{-4}$ cm^2 for 0·6 cm beads. These values are reliable to within 5 %.

Experimental method

To begin each experiment a two-layer salinity distribution was established in the fluid within the porous medium, with the upper layer initially of fresh water. It was desirable to achieve contact between the glass medium and inner Al plate when the lid was sealed into position, although there sometimes remained a fluid space about 0·1 cm deep. Heating and cooling were turned on and the first samples were withdrawn after the two layers had reached roughly constant temperatures. Thereafter the sampling periods varied from 3 to 20 hours. Samples were taken from the centre of each layer simultaneously and up to twenty 1 ml samples were taken from a single experiment. At most 0·1 % of the fluid volume was withdrawn at each sampling time.

Injection of dye allowed visualization of the cell geometries and interface position near the walls of the box. However, when the interface was observed to be planar, a more accurate determination of interface position (and therefore of layer volumes) could be obtained from the vertical temperature profile near the centre of the box. Experiments were terminated whenever fluid from one layer reached the resistance thermometer in the opposite half of the box either due to migration of the interface (see § 6) or to complete overturning of the fluid.

6. Experimental results

The convection

A single thermal Rayleigh number, $\bar{R}_m$, for the thermohaline systems can be defined in terms of the mean layer depth $\bar{H}$, the temperature difference ΔT between average layer temperatures, a mean viscosity for the system, $\bar{\nu} = \nu(\bar{T}, \bar{S})$, and a mean coefficient

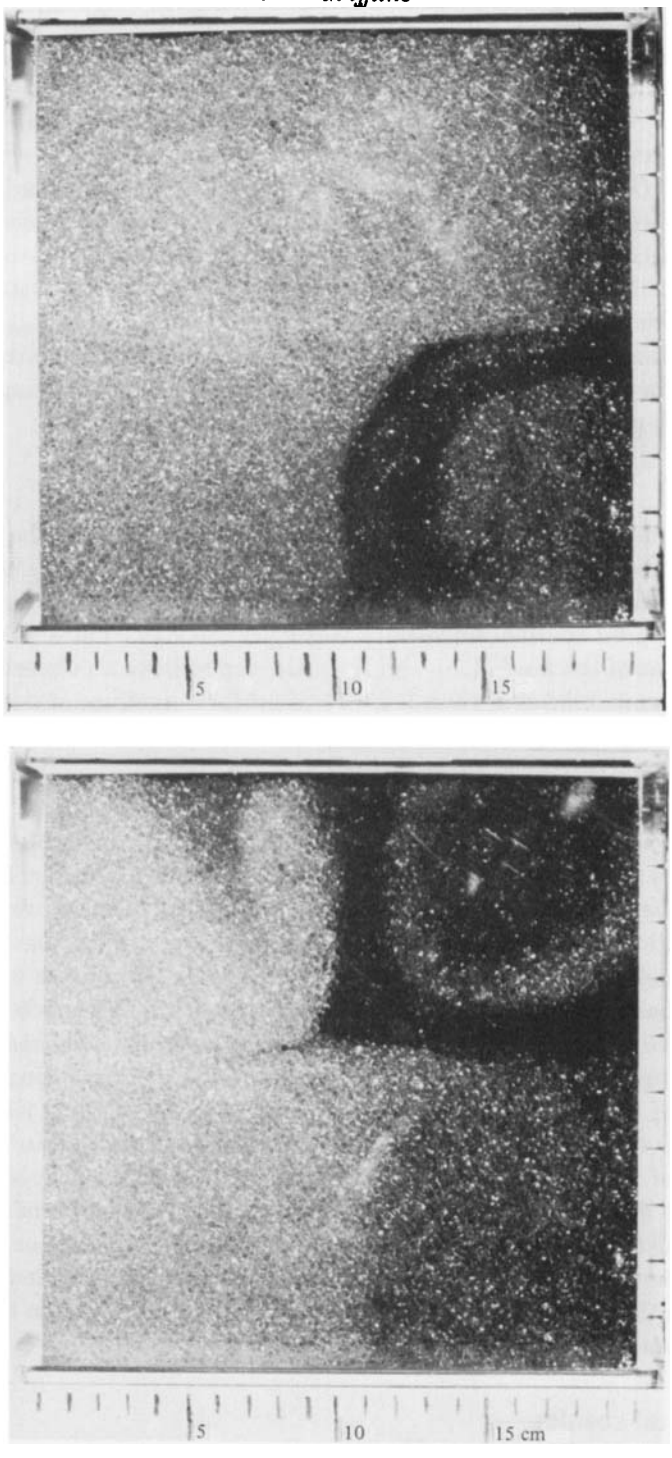

FIGURE 4. Photographs of one wall of box B showing layered convection. Frame (*a*) was taken 13 min after dye was injected near the right-hand wall (red in the lower layer, blue in the upper layer). Frame (*b*) was taken 110 min later when the red dye had mixed through half of the lower layer and blue dye was mixing through the upper layer. There are 4 cells along each of the four walls in each layer. $R_\rho \approx 2{\cdot}7$, $\bar{R}_n \approx 450$ (experiment (*d*)).

Experiment	Box	l	Symbol	$\bar{R}_m$	R_u	R_l
(*a*)	*A*	0·3	◇	510	160	820
(*b*)	*A*	0·3	□	630–690	290–330	1190–1940
(*c*)	*A*	0·3	△	510–700	250–340	940–1700
(*d*)	*B*	0·3	○	400–470	110–150	760–1050
(*e*)	*B*	0·3	▽	230–260	220–270	410–430
(*f*)	*A*	0·6	●	1620–2060	200–360	1030–3320
(*g*)	*B*	0·6	■	1060–1130	100–140	890–1070
(*h*)	*B*	0·6	▲	1050–1230	180–230	830–1240
(*i*)	*B*	0·6	▼	580–750	—	390–510

TABLE 1. Rayleigh numbers for thermohaline experiments in a porous material. The bead diameter is l (centimetres). The symbols are to be referred to the figures.

of thermal expansion, $\bar{\alpha} = \alpha(\bar{T}, \bar{S})$ where $\bar{T}$ and $\bar{S}$ are the mean temperature and salinity across the interface. In order to calculate the Rayleigh number, the density ratio R_ρ and the buoyancy flux αF^P, the value of $\alpha = (1/\rho)\,\partial\rho/\partial T$ was found from the polynomials presented by Ruddick & Shirtcliffe. The resulting mean Rayleigh numbers spanned the range $230 < \bar{R}_m < 2000$. However, different Rayleigh numbers, R_u and R_l, are appropriate to the convection in the upper and lower layers respectively. These are based upon the local values of α, ν and H and upon an effective temperature drop across the convecting layer. The value of α was as much as a factor of 3 greater, and that of ν a factor of 2 smaller, in the lower layer than in the upper layer. The effective temperature drop was assumed to be twice the measured temperature drop, T', between the inner Al plates and the averaged centre of the adjacent layer.

In table 1 are listed estimates of $\bar{R}_m$, R_u and R_l for each heat–salt experiment. The box in which the experiment was performed and the bead diameter are also shown, along with a symbol that will be used to show data points in later figures. The large difference between the Rayleigh numbers for individual layers explains some observed properties of the convection. In figure 4 are shown photographs of one side of box B. The dye movements indicate that cell aspect ratios were smaller in the lower layer ($0{\cdot}2 < L/H < 0{\cdot}7$) than in the upper layer ($0{\cdot}5 < L/H < 1$). Reynolds numbers (based on l) ranged from 3×10^{-2} in the lower layer to 1·2 in the upper layer. If the influence of salinity gradients within each layer is neglected, we can also find the thermal boundary-layer thickness, δ, from $\delta/H \sim Nu^{-1} \gtrsim 10^{-1}$. Then $\delta \sim 1$ cm, which is larger than the grain size.

Once dye became mixed throughout a layer it revealed the interface position and two significant observations were made. First, the interface slowly migrated upward, implying a net downward exchange of fluid into the lower layer. Indeed, streaks of dye from the upper layer could sometimes be seen in the lower layer. A similar behaviour was noted by Marmorino & Caldwell (1976) for the viscous fluid case. The second observation was that the interface was planar and horizontal at $R_\rho > 3$ but became distorted when $R_\rho < 2$ (only small distortions can be seen in the photograph shown in figure 4*b*). They appeared to have a horizontal wavelength of $2L$, where L is the width of one convection cell. Their amplitude became comparable to $2L$ at $R_\rho < 1{\cdot}5$. A warm plume existed on *both* sides of the interface at its highest points and cold plumes at its lowest points, a behaviour that is common to two-layer heat–salt systems in the laboratory (Griffiths 1979).

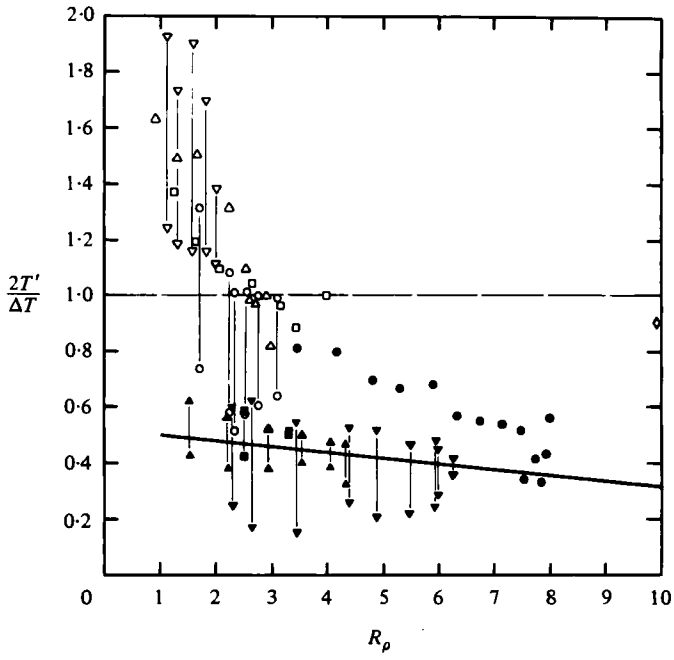

FIGURE 5. The measured temperature drop, T', from the inner Al plate thermistor to the horizontal average near the centre of the adjacent layer, normalized by half the temperature drop ΔT between layers. Curves $2T'/\Delta T = 1$ and $2T'/\Delta T = \frac{1}{2}(\delta T/\Delta T)$ are shown. Symbols are those defined in table 1 and the points obtained simultaneously from upper and lower layers in box B are connected.

Further evidence of an increased interfacial surface area is shown in figure 5, where the quantity $2T'/\Delta T$ is plotted against R_ρ. As before, T' is the measured temperature difference between the inner metal plate and the horizontally averaged temperature at the centre of the adjacent layer. Simultaneous results from the lid and base of box B are connected. (There is a large uncertainty in T' as it is the difference between a horizontal average for the fluid temperature and a local measurement in a metal plate which contains significant temporal and spatial variations.) It is reasonable to assume that the thermal boundary layers on each side of a convecting layer are identical when the interface is planar. Therefore we again assume $2T'$ to be the temperature drop that drives convection in a layer. However, $2T'$ then has a maximum possible value of ΔT. On the other hand, most experiments indicate that $2T' > \Delta T$ when $R_\rho < 2$. These are the density ratios at which interface distortion was observed.

The data of figure 5 have further significance. In obtaining the dimensionless heat flux (9) it was assumed that the effective temperature drop across each layer was $\frac{1}{2}\delta T$. For planar interfaces we now write $2T' = \frac{1}{2}\delta T$ and obtain the relation

$$2T'/\Delta T \simeq \tfrac{1}{2}(\delta T/\Delta T),$$

where $\delta T/\Delta T$ is given by (8) and (6). The curve is plotted in figure 5 and is consistent with the temperature measurements at $R_\rho > 3$. These are the density ratios at which the interface was observed to be planar. At smaller density ratios, measurements obtained with the smaller bead size ($l = 0{\cdot}3$ cm) lie well above the plotted curve while

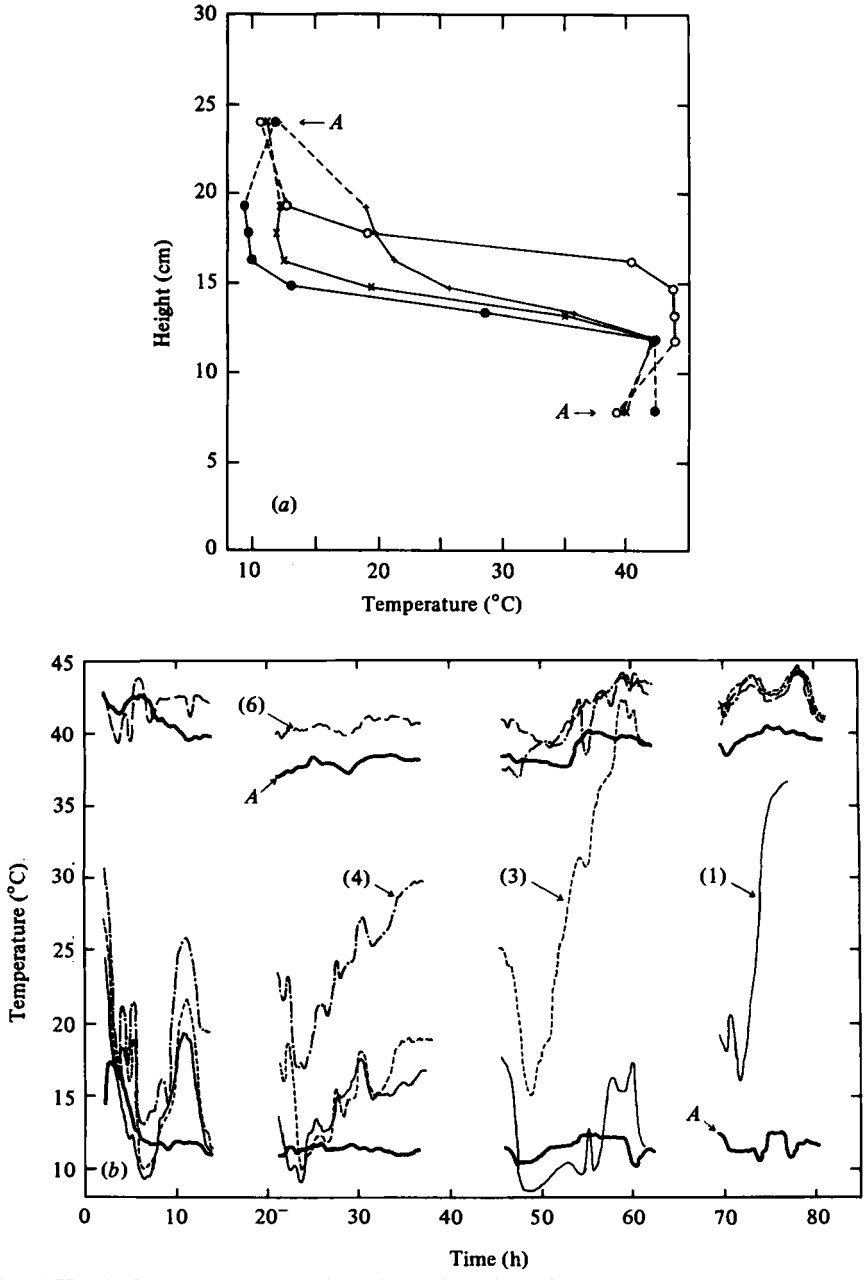

FIGURE 6. (*a*) Vertical temperature profiles through an interface and (*b*) temperature *versus* time records from some of the thermistors for the same experiment (experiment (*f*)). The upper and lower points marked *A* in (*a*) and the heavy lines in (*b*) are the horizontally averaged temperatures. In (*a*), times in hours from the beginning of the experiment are: ●, 6·5; +, 11; ×, 13; ○, 60·5. Thermistor numbers from the top of the array are shown in (*b*). Despite the observed fluctuating behaviour, layer temperatures were constant over long periods and interface migration is obvious.

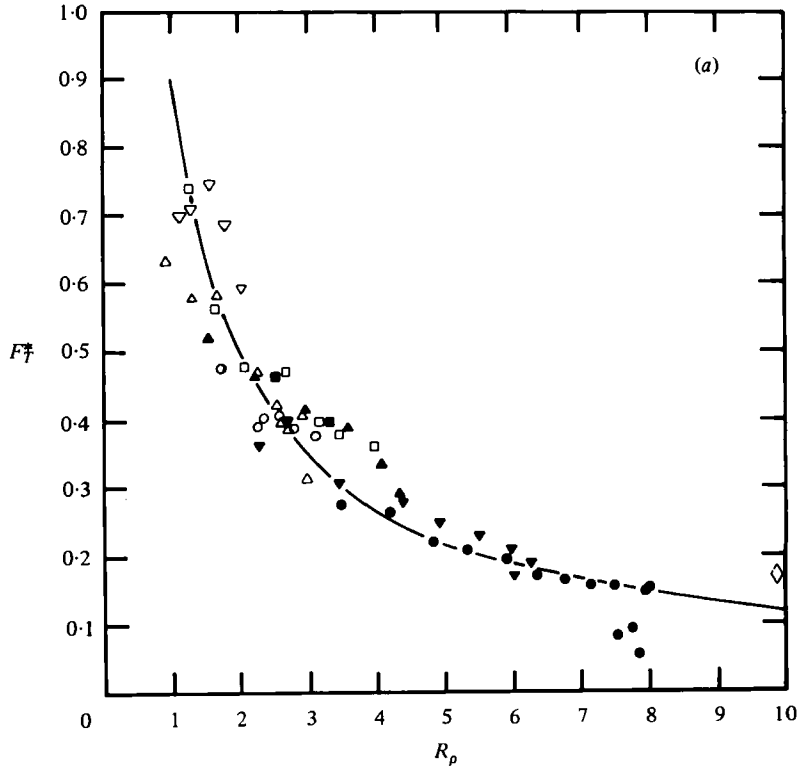

FIGURE 7(a). For legend see facing page.

those obtained with $l = 0{\cdot}6$ cm are more consistent with the curve. More data are needed in order to see whether this dependence upon bead size is real.

Vertical temperature profiles obtained from the thermistor array revealed the interface position while it was planar. In figure 6(*a*) are shown examples of vertical profiles taken from the temperature record of which a part is shown in figure 6(*b*). The point measurements are also compared to the horizontally averaged layer temperatures. Temperature maxima and minima often occurred at the edges of an interface and imply the presence of unsteady convective motions. Upward migration can be seen and an estimate of the interface thickness, h, is possible. The quantity

$$h = \Delta T/(dT/dz)_{\max},$$

based on the maximum temperature gradient detected within the interface, varied from 3 cm at $R_\rho = 8$ to approximately 0·6 cm at $R_\rho = 3$. Fluctuating temperatures were characteristic of most experiments and the record shown in figure 6(*b*) illustrates that fluctuations were detected by both the averageing thermometers and the thermistors. This behaviour was a significant cause of scatter in the heat-flux measurements since the inner Al plates did not reach a uniform temperature but partially responded to the local fluid temperature. Fluctuating thermal convection was detected in laboratory porous medium experiments by Combarnous & LeFur (1969), and Caltagirone, Cloupeau & Combarnous (1971).

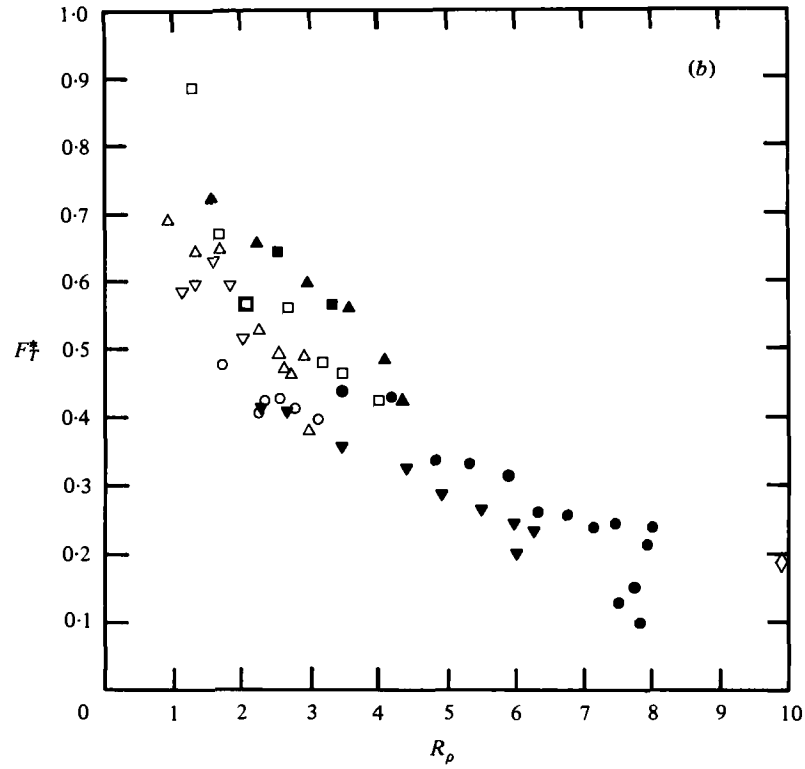

FIGURE 7. The dimensionless heat flux, $F_T^* = F_T/F^P$, from the porous medium experiments plotted against the density ratio $R_\rho = \bar{\beta}\Delta S/\bar{\alpha}\Delta T$. In (*a*) the normalizing heat flux F^P is found from the $\frac{2}{3}$-power law of (2), but in (*b*) from the $\frac{1}{3}$-power law of (1). Normalization with the $\frac{2}{3}$-power law collapses the data most efficiently, making the heat flux independent of Rayleigh number.

The heat flux

Measurements of the heat flux, F_B, through the base and lid were averaged over the period between salinity samples. The heat flux, F_T, through the interface was then obtained by subtracting the expected side-wall heat loss from F_B. The latter ranged from 6×10^{-3} to $3{\cdot}6\times10^{-2}$ cal cm^{-2} s^{-1} and the rate of side-wall loss was at most 3 % of the rate of heat addition through the base for tank B, but sometimes reached 25 % for tank A. A further correction for interface migration was only significant when $R_\rho < 3$, while a correction for unsteady average temperatures was usually negligible. The vertical heat transport contains a contribution of 1–4 % due to the finite conductivity of the Perspex walls. For box B, the calculated interfacial heat fluxes given by the base and lid HFMs were always within 10 % of each other and only the mean of the two values will be discussed.

In order to find the appropriate 'solid plane' heat flux, F^P, measured values of ΔT between layers were used in the Nusselt number relation (2). The density step $\bar{\alpha}\Delta T$ and buoyancy flux $\bar{\alpha}F^P$ were based on the coefficient $\bar{\alpha} = \alpha(\bar{T},\bar{S})$. In figure 7(*a*) are shown the resulting dimensionless heat fluxes, $F_T^* = F_T/F^P$. Normalizations of F_T using both the linear Nusselt–Rayleigh number relation and the asymptotic $\frac{1}{3}$-power

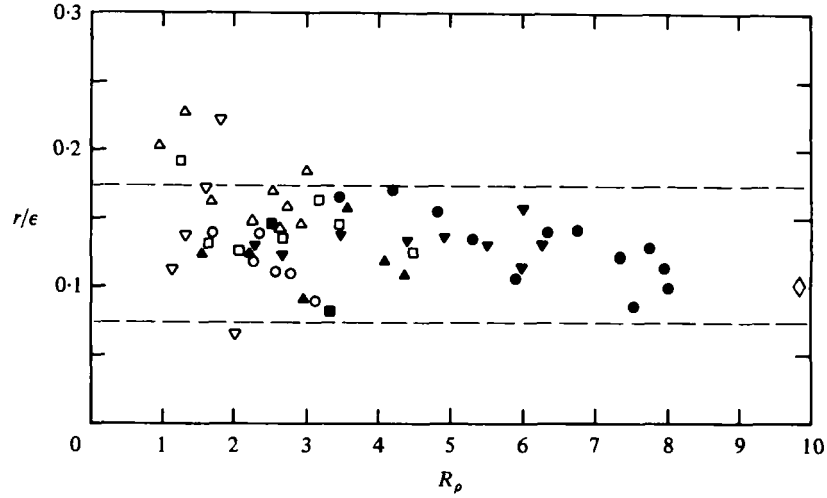

FIGURE 8. The ratio r of buoyancy fluxes due to salt and heat obtained from the experiments, normalized to its value at a porosity of $\epsilon = 1$ (i.e. a viscous fluid). The experimental medium of glass spheres had a porosity of $\epsilon = 0{\cdot}38$. The lower broken line shows the value of $\tau_m^{\frac{1}{2}}$ and the upper line (discussed in §7) shows its modified value when mechanical dispersion is included.

law of (1) were also tested. The dimensionless heat fluxes using (1) are plotted in figure 7 (*b*). It can be seen that the $\frac{2}{3}$-power law of (2) collapses the data for the experimental range of Rayleigh numbers. The other normalizations resulted in a much greater scatter of F_T^*. No systematic errors are apparent in each experiment since the many experiments and the results from two boxes agree. The data show no dependence of the heat flux upon bead size. The simple power law that best describes the data of figure 7 (*a*) is

$$F_T^* = MR_\rho^{-N}, \tag{10}$$

where $M = 0{\cdot}90 \pm 0{\cdot}03$ and $N = 0{\cdot}89 \pm 0{\cdot}07$.

The ratio of salt and heat buoyancy fluxes

The mass flux of salt, F_S, through the interface was calculated from the concentration change in the top layer between sampling times, knowing the mean depth ϵH_u of the water column. A density flux $\bar{\beta}F_S$ was then defined in terms of the coefficient

$$\bar{\beta} = (1/\bar{\rho})\,\partial\rho\,(\bar{T}, \bar{S})/\partial S.$$

The resulting values for the ratio of salt and heat density fluxes, divided by the porosity, are shown in figure 8. These data are to be compared with (6). As predicted, the empirical flux ratio shows little dependence upon R_ρ, although there is a small increase of r at small density ratios ($R_\rho < 3$). There is no dependence upon either the Rayleigh number or bead size. Mean experimental temperatures of 33 °C imply a salt diffusivity of $\kappa_s \simeq 2 \times 10^{-5}\,\mathrm{cm^2\,s^{-1}}$ and a diffusivity ratio of $\tau_m = 5{\cdot}2 \times 10^{-3}$ (± 15 %). Therefore $\tau_m^{\frac{1}{2}} = 0{\cdot}072 \pm 0{\cdot}006$, and this value is shown as the lower line in figure 8. The data give a mean value of $r/\epsilon = 0{\cdot}14 \pm 0{\cdot}03$ which is twice the suggested value of $\tau_m^{\frac{1}{2}}$. The upper broken line in the figure will be discussed in §7.

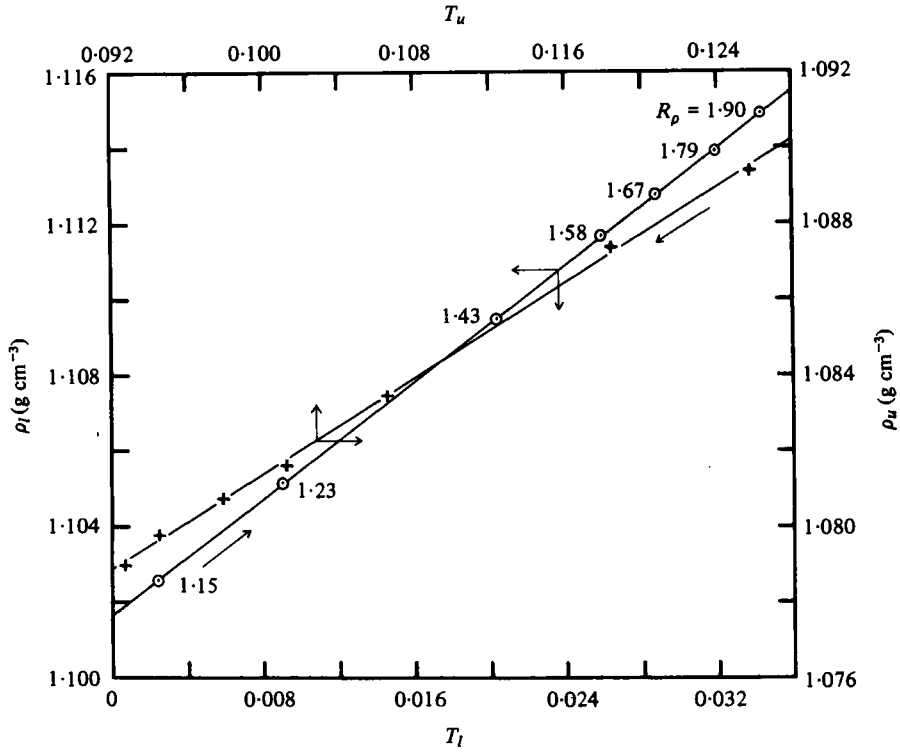

FIGURE 9. The two-layer salt–sugar system in the porous medium: a linear relation between the layer densities and salt concentrations as they change due to fluxes across the interface. Subscripts u and l refer to upper and lower layers. The directions of 'run-down' are indicated.

The salt–sugar system

When the porous medium was saturated by a layer of salt solution above a layer of sugar solution, injected dye again revealed convective motions within each layer. In this case the motions appeared to take a much smaller aspect ratio ($L/H < 0{\cdot}2$). The system ran down from an initial density ratio of $R_\rho = 1{\cdot}15$ to $R_\rho = 1{\cdot}90$ over a period of 200 hours.

In order to find the ratio of buoyancy fluxes, r, note that conservation of mass requires the fluxes to satisfy the relation

$$\alpha F_T \left(1 - \frac{\beta F_s}{\alpha F_T}\right) = \epsilon \frac{d}{dt}(H\rho) \tag{11}$$

within each layer. The coefficients α and $\beta(T, S)$ take local values in each layer and these values may be calculated from the polynomials of Ruddick & Shirtcliffe. Thus two different values of r can be found by substituting $F_T = \rho\epsilon H(dT/dt)$ into (11), assuming the layer depth H to be constant, and applying the result

$$\frac{d\rho}{dT} = \rho\alpha(1-r) \tag{12}$$

to the upper and lower layers. Relation (12) is fitted to the data points for one experiment in figure 9. It yields a constant slope because there is only a small change with

time of $\rho\alpha (= \partial\rho/\partial T)$ in each layer. At the same time, a nonlinear equation of state and a variable layer depth both allow $r = \beta F_S/\alpha F_T$ to take unequal values in the two layers (Griffiths & Ruddick 1980). The mean flux ratio is $r = 0{\cdot}55 \pm 0{\cdot}03$, a value that falls close to the predicted value of $\tau^{\frac{1}{2}} = 0{\cdot}57 \pm 0{\cdot}02$ (remember that both components are confined to the fluid space in a two-solute system).

The results that have been presented in this section are discussed in § 7. They are compared with the theoretical predictions of § 4 and with results previously obtained for the 'diffusive' interface in a viscous fluid. The flux ratio and dimensionless heat flux will be discussed individually.

7. Discussion of experimental results

Flux ratio

The ratio of buoyancy fluxes will be considered first. Over most conditions (R_ρ not too close to 1) the flux ratio is independent of all parameters tested in the laboratory except the ratio of diffusion coefficients. The value of r for a two-solute 'diffusive' interface in a porous medium is found to be close to $\tau^{\frac{1}{2}}$. A similar flux ratio, $r = 0{\cdot}60 \pm 0{\cdot}01$, was found for the analogous salt–sugar interface in an unconstrained viscous fluid (Shirtcliffe 1973). The measured flux ratio for thermohaline interfaces in a porous medium also has some behaviour in common with the viscous fluid case. In particular, the qualitative agreement with (6) provides some support for the description of the coupling between layer convection and diffusion through the interface in terms of an intermittent boundary-layer flow. However, there are two significant differences between the two thermohaline systems. First, there is a rapid increase of the flux ratio at $R_\rho < 2$ in Turner's (1965) experiments. In that system, inertial fluid motions are able to alter the nature of transport through the density interface (Linden 1974). Inertial effects are negligible in the porous medium experiments. Second, the magnitude of the flux ratio at $R_\rho > 2$ is twice its estimated value for the experiments reported in this paper, while the ratio ($r = 0{\cdot}15$) for the unconstrained fluid interface is only slightly greater than $\tau^{\frac{1}{2}} (= 0{\cdot}11)$. A possible explanation of this difference follows.

Viscous entrainment of non-buoyant fluid from the interface edges was suggested as the cause of a flux ratio greater than $\tau^{\frac{1}{2}}$ across a viscous fluid interface (Linden & Shirtcliffe 1978). However, another process can increase the transport of solute within a porous material. In the experiments reported in § 5 the observed convection velocities, U (averaged between layers), indicate Péclet numbers of $50 < Ul/\kappa_s < 200$ and $0{\cdot}5 < Ul/\kappa_m < 2$. As before, l is a characteristic pore dimension. Thermal gradients are therefore small but salinity gradients may be high within individual pores. Mechanical dispersion can therefore significantly increase the effective diffusion coefficient of the solute. Dispersion experiments in a bed of glass spheres (see Saffman 1960) suggest an effective diffusion coefficient at the above Péclet numbers of $D^* \sim 4\kappa_s$ (but no mechanical dispersion of heat). Then D^* replaces $D = \frac{2}{3}\kappa_s$ in (6). The modified diffusivity ratio gives $\tau_m^{\frac{1}{2}} \sim 0{\cdot}18$ which is shown as the upper line in figure 8. It forms a good upper bound for the data and indicates that, if we accept the arguments leading to (6), this form of 'entrainment' at the interface edge can explain the observed flux ratio.

Heat flux

The dimensionless heat-flux data of figure 7 (*a*) show no dependence upon the Rayleigh number of the convection or upon bead size. These data have been fitted by the curve (10), which reveals a behaviour similar to that of Huppert's (1971) approximation to the dimensionless heat flux through a viscous fluid interface: $F_T^* = 3{\cdot}8R_\rho^{-2}$. In the porous medium case, though, we have already seen that the fluid convection is unable to supply energy to inertial motions at the interface and, as a result, mechanical mixing is negligible. This explains the only significant difference between the two empirical heat-flux curves: the interfacial heat flux F_T exceeds the 'solid plane' heat flux as $R_\rho \to 1$ in the unconstrained fluid, while the heat flux through a 'diffusive' interface within the laboratory porous media is always less than the appropriate 'solid plane' flux.

It is also known that $F_T^* > 1$ in the unconstrained two-solute system when $R_\rho \to 1$ (Shirtcliffe 1973). In this case, the larger salt and sugar fluxes might be attributed to an increased interfacial surface area produced by inertial fluid motions that distort the density interface. No breaking waves or penetration of the interface by 'thermals' are observed in such a system (possibly owing to a zero buoyancy flux through the top and bottom of the laboratory system). This is consistent with the observation that salt and sugar buoyancy fluxes remain in a constant ratio as $R_\rho \to 1$. In a similar way the layer convection in both thermohaline systems visibly distorts the density interface (though not by inertial forces in the porous medium case) and the resulting increased surface area will again influence the heat and salt transport.

To assess the influence of interface bending upon the vertical heat flux in the porous medium case, an upper limit for the surface area change can be estimated. Assume all distortions to be sinusoidal in two dimensions (a reasonable approximation to laboratory observations), with an amplitude η and wavelength $2L$. When $\eta < L$ it can be shown that such a surface has an area A given by

$$\frac{A}{A_B} \sim 1 + 2\left(\frac{\eta}{L}\right)^2, \tag{13}$$

where A_B is the cross-sectional area of the box.

The amplitude of the distortion is determined by a combination of horizontal property variations (T'') in each convecting layer and the pressure gradient ($\Delta P/L$) necessary to force horizontal flow between up- and down-going plumes. Here, T'' is defined as the mid-layer departure of T from its horizontal mean value ($T'' \sim \frac{1}{4}.\frac{1}{2}\delta T$). Horizontal salinity variations are neglected since the flux ratio $r \sim 0{\cdot}05 \ll 1$. At this stage it is assumed that the interface distortion does not itself greatly influence the convection. To find a maximum distortion for given average layer properties the cell configuration sketched in figure 10 is considered, with flow along the interface assumed to be quasi-horizontal. From Darcy's law, the horizontal flow velocity is

$$U \simeq \frac{k}{\rho\nu}\frac{\Delta P}{L}, \tag{14}$$

and the corresponding pressure difference between plumes is

$$\Delta P \simeq 2\eta g\Delta\rho - 2(H + 2\eta)\, g\rho\, |\alpha T''|, \tag{15}$$

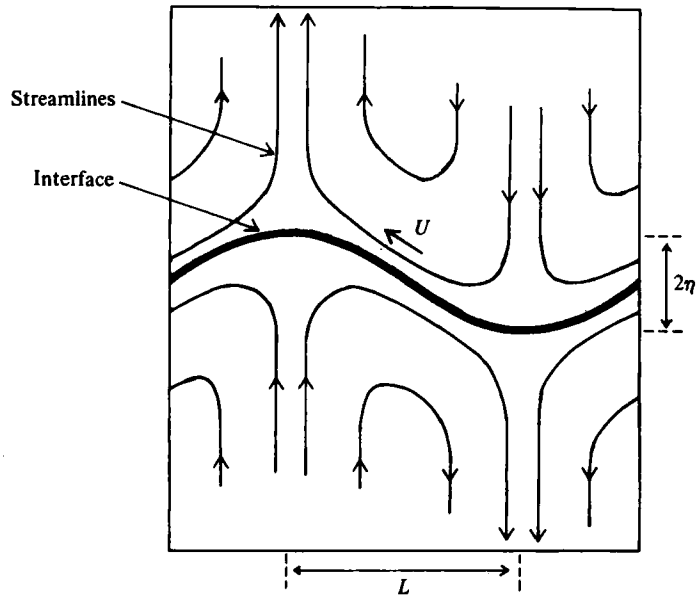

FIGURE 10. A sketch of the convection geometry that would give the maximum interface curvature. Cells in the upper and lower layers are of the same horizontal dimension.

where $\Delta\rho$ is the difference between average layer densities. In order to be consistent with the use of (2), the horizontal boundary-layer velocity and vertical plume temperature for thermal convection are given by

$$\alpha T'' \simeq (\alpha\delta T/8)\,(R_m/40)^{-\frac{1}{3}}, \quad U \simeq 11(\kappa_m/H)\,(R_m/40)^{\frac{2}{3}}. \tag{16}$$

These relations are obtained from the analysis of Robinson & O'Sullivan (1976) and, although the Rayleigh number dependence may not be accurate, they lead to useful qualitative predictions. From (14)–(16) the amplitude becomes

$$\frac{\eta}{L} \sim 0{\cdot}29\left(\frac{R_m}{40}\right)^{\frac{2}{3}}\left(\frac{18{\cdot}7R_m^{-1}+\phi}{R_\rho-1-\phi}\right), \tag{17}$$

where $\phi = \frac{1}{4}[(1-\tau_m^{\frac{1}{2}}R_\rho)/(1-\tau_m^{\frac{1}{2}})]\,(R_m/40)^{-\frac{1}{3}}$. The fractional increase of interface area may now be found as a function of R_ρ and R_m by substituting (17) into (13). Then an upper bound to the heat flux is obtained by assuming that F_T is increased above that through a planar interface by this same fraction. Of course, the full increase cannot be realized as one boundary of each convecting layer remains planar.

In figure 11 are reproduced the dimensionless heat-flux data of figure 7 (a). These are compared to the heat flux predicted by (8) and (9) (solid line) using the empirical value of r and to the modification of this prediction due to the surface-area correction (broken lines). Equation (9) provides an excellent description of the data for $R_\rho > 3$, an agreement which indicates that the equation is based upon the correct temperature drop ($\frac{1}{2}\delta T$) across each layer.

A comparison between the porous-medium results and the dimensionless heat-flux

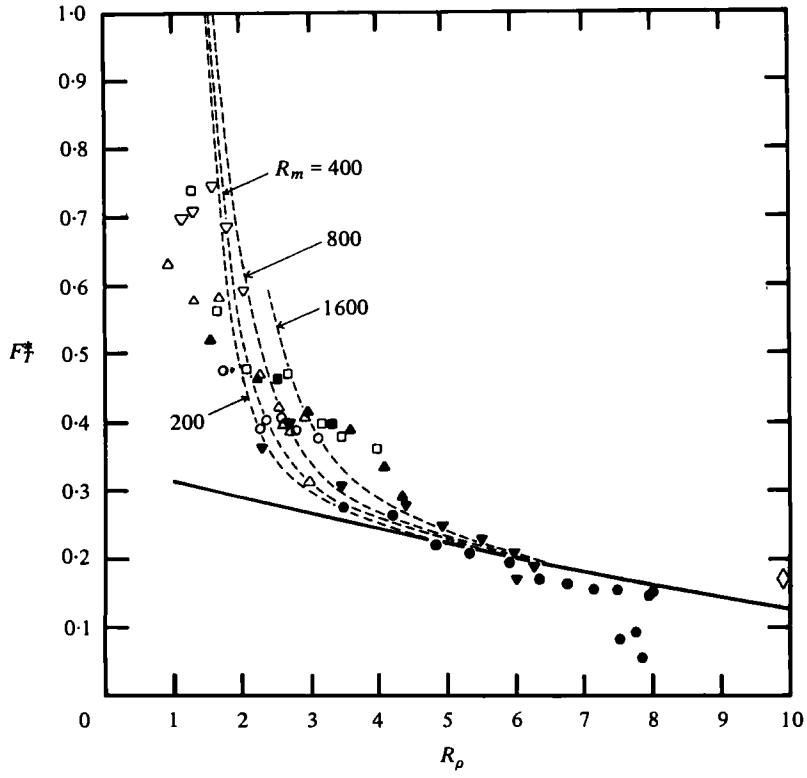

FIGURE 11. Dimensionless heat-flux data of figure 7 (*a*) for the 'diffusive' interface in a medium of glass beads, compared with the prediction of equations (8) and (9) (solid curve). The broken curves are upper bound estimates including the influence of interface curvature for several Rayleigh numbers.

data for the viscous fluid interface is useful here. The data of Turner (1965) for a heat–salt interface are shown in figure 12. In place of equation (9), the solid curve is this time

$$F_T^* = \left(\frac{1}{2}\frac{\delta T}{\Delta T}\right)^{\frac{4}{3}} \tag{18}$$

and the analogous relation to (6) is $\delta T/\Delta T = (1-\tau^{\frac{1}{2}}R_\rho)/(1-\tau^{\frac{1}{2}})$. Equation (18) is obtained by writing the Nusselt number relation for high Rayleigh number thermal convection of a viscous fluid in each layer in the form $2F_T H/(\kappa_T \delta T) = cR^{\frac{1}{3}}$. The 'solid plane' Nusselt number is $F^P H/(\kappa_T \Delta T)$ and the effective temperature drop is again assumed to be $\frac{1}{2}\delta T$. The broken curve is that given by the complete interface model of Linden & Shirtcliffe, and is based on a quantitative description of the boundary-layer instability. The agreement between the two curves and the data of figure 12 indicates the usefulness of our simple description of the layer convection in terms of previous knowledge of the heat flux through purely thermal convection. However, it should be remembered that the assumption of highly unsteady, intermittent convection in a porous medium overlooks the existence of plumes which occupy a large fraction of a layer volume and the presence of significant horizontal T and S variations along the interface edge. Such inhomogeneities made it necessary to define ΔT as

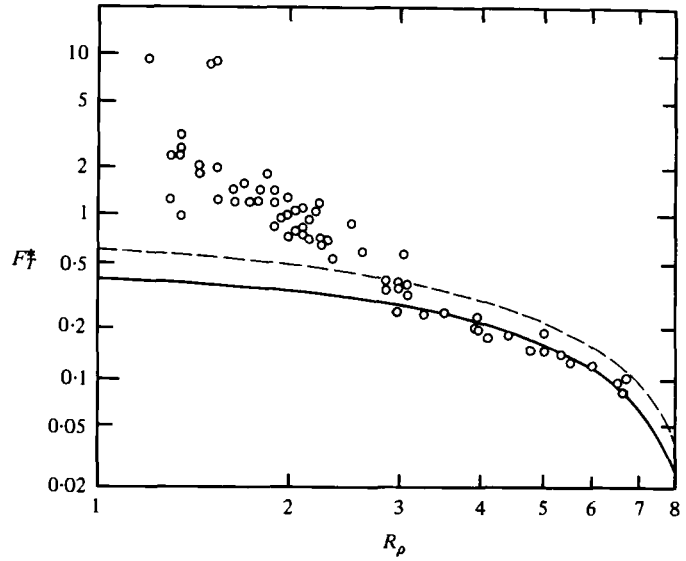

FIGURE 12. Dimensionless heat-flux results for the viscous fluid 'diffusive' interface (from Turner 1965). The broken curve is that predicted by Linden & Shirtcliffe (1978). The solid curve is equation (18) and is the result that corresponds to the solid curve shown in figure 11 for the porous medium case. Both curves provide a good description of the data for $R_\rho > 3$.

the difference between mid-layer horizontal temperature averages in the experiments. It is not clear how this is consistent with the definition in § 4, where ΔT is again the difference between average layer temperatures but where the buoyant fluid (warm plumes) occupies a negligible volume of a convecting layer.

From figures 11 and 12 we conclude that, when $R_\rho > 3$, the interfaces in both types of layered thermohaline convection act as rigid boundaries. Further, the upward flux of solute does not significantly reduce the heat-transporting capacity of the thermal convection in each layer. This was to be expected as only 5% of the potential energy released from the temperature field in the porous medium experiments is used to raise the centre of gravity of the salinity field.

At smaller interfacial stabilities, $R_\rho < 3$, the curves on figure 11 show that the estimated upper bounds for the influence of interface distortion can reconcile relation (9) with the measured heat fluxes. These are also the conditions under which the interface was observed to be non-planar and under which $2T' > \Delta T$. For Rayleigh numbers in the range $200 < \bar{R}_m < 1600$, the estimated amplitude of the interface distortions reaches $\eta \sim \frac{1}{2}L$ at density ratios in the range $2{\cdot}3 < R_\rho < 3$. This too agrees with dye observations. At still lower density ratios the density step, $\Delta\rho$, across the interface decreases more rapidly than the density anomaly between vertical plumes, causing $\eta/L \to \infty$ at $R_\rho \sim 1{\cdot}1$. For $R_\rho < 1{\cdot}1$ it is predicted that two layers cannot exist indefinitely. Within the box, though, rigid top and bottom boundaries will reduce the interface distortion. Further, even when measurements showed that $2T' > \Delta T$, the normalized heat flux F_T^* did not reach unity. This implies that the heat-transporting capacity of the layer convection at low density ratios was reduced by either salt transport or interface curvature.

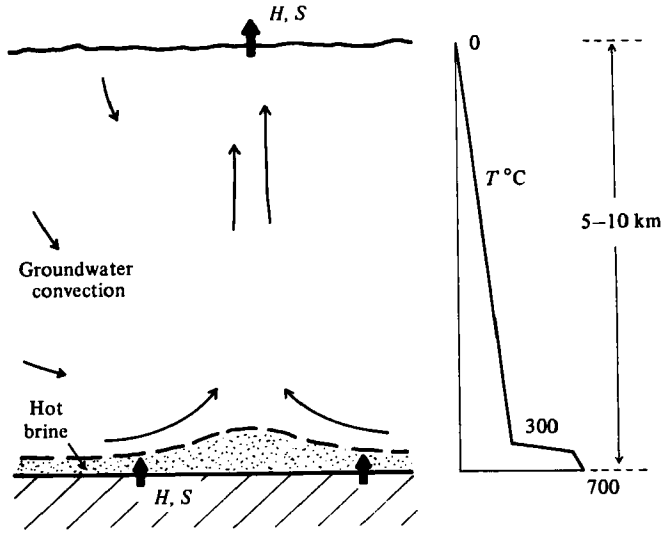

FIGURE 13. An idealized model for the Wairakei geothermal system. The motion of groundwater near a hot plume is illustrated. A denser layer of hot saturated brine insulates the heat source and a 'diffusive' thermohaline interface separates the brine from the groundwater (broken line). Heat (H) and salt (S) are supplied from the magma body and released at the ground surface.

8. Geothermal systems

Some implications of double-diffusive convection within the Earth's crust are best discussed in terms of an example. McNabb (1975) has already suggested the possible existence of two fluid layers in the Wairakei geothermal field of New Zealand. He suggests that saline magmatic fluid released from the 'hot plate' beneath the hydrothermal system may boil and give rise to a fluid saturated with solutes. As most of the circulation (5–10 km deep) consists of dilute (2‰) groundwater, the hot, saturated brine (200‰) is more dense and may form a layer at the bottom. This would then insulate the groundwater from the high-temperature regions exceeding 400 °C.

The model system suggested by McNabb, and to which the ideas that have been developed in this paper will be applied, is illustrated in figure 13. While the groundwater does not reach temperatures greater than 300 °C, the lower boundary is thought to be close to 700 °C. This leaves a temperature drop of about 400 °C which must be accommodated across the proposed brine layer and its interface with the groundwater. If we assume that a temperature drop of 200 °C is available to drive convection within a brine layer that is 10^4 cm deep, the values $k \sim 10^{-10}\,\mathrm{cm}^2$ (McNabb, Grant & Robinson 1975), $\alpha\Delta T \sim 10^{-1}$, $\nu \sim 10^{-3}\,\mathrm{cm}^2\mathrm{s}^{-1}$ and $\kappa_m = 3\times10^{-3}\,\mathrm{cm}^2\mathrm{s}^{-1}$ imply a thermal Rayleigh number of $R_m \sim 30$. Therefore, the groundwater circulation may well be supplied with heat and salt through a lower convecting layer of brine and diffusion through a stable interface. The groundwater circulation has $H \sim 5$ km and $R_m \sim 10^3$. The system can remain in a steady state due to expulsion of heated groundwater at the surface, intake of fresh meteoric water and a continuous input of magmatic fluid from below.

The buoyancy fluxes due to both heat and salt through the brine/groundwater interface may be estimated from measured quantities. The geothermal field (150×20 km) consists of many hot plumes of area 10 km^2. Each plume carries 5×10^7 cal s^{-1} and about 400 g s^{-1} of salt at a concentration of 1‰ to 2‰. Using the conditions near the postulated brine/groundwater interface (500 bars, 500 °C, 100‰; $\alpha \sim 10^{-3}$ °C^{-1}, $\beta \sim 2$, $C_p \sim 2$ cal g^{-1} °C^{-1}) the ratio of salt to heat buoyancy fluxes becomes, within a factor of 3, $\beta F_s/\alpha F_T \sim 0{\cdot}03$. Any effects of boiling are neglected.

A flux ratio can also be predicted from (6) if both layers are convecting, since the postulated density interface will be of the 'diffusive' kind. McNabb has estimated the diffusion coefficient for sodium chloride in water at the conditions of interest to be $\kappa_s \simeq 2 \times 10^{-4}$ cm^2 s^{-1}. The estimated porosity is $\epsilon = 0{\cdot}2 \pm 0{\cdot}1$. Then

$$r = \epsilon(\tfrac{2}{3}\kappa_s/\kappa_m)^{\frac{1}{2}} \simeq 0{\cdot}04 \pm 0{\cdot}02,$$

which is equal to the 'observed' flux ratio to well within the uncertainty of either value.

The presence of a 'diffusive' interface would also have implications for the heat flux through the geothermal system. Individual contributions to the density step in the present example are estimated to be $\alpha\Delta T \sim 0{\cdot}1$ and $\beta\Delta S \sim 0{\cdot}4$, giving a density ratio of $R_\rho \sim 4$. From the results of laboratory experiments reported in § 6 the heat flux through the system would be approximately $\frac{1}{4}$ of the 'solid plane' flux based on the temperature difference, ΔT, between layers. Furthermore, ΔT is less than the total temperature drop across the system (and the 'solid plane' heat flux is roughly proportional to a $\frac{5}{3}$ or $\frac{4}{3}$ power of the temperature drop across a convecting layer). It must therefore be concluded that the heat flux through an interface, assuming a fixed medium, would be an order of magnitude less than that given by direct thermal convection between the 'hot plate' and the surface. This suggests that permeability estimates based upon heat flow observations (McNabb *et al.*) might be nearly an order of magnitude too small since the calculations have assumed simple thermal convection. The thermal Rayleigh numbers for each layer would then be greater. More significantly, the layered convection suggested here would decouple the salt flux into the groundwater from the magmatic supply of heat and salt. A 'diffusive' interface maintains, but allows interaction between, two different chemical and thermal environments.

9. Conclusions

Experiments with a two-layer convecting system in a Hele-Shaw cell and a porous medium of glass spheres indicate that a thin 'diffusive' density interface is maintained against diffusive thickening, despite the lack of inertial forces. The ratio of salt to heat buoyancy fluxes through the interface in the laboratory experiments is given to a reasonable approximation by $r = \epsilon\tau_m^{\frac{1}{2}}$, where ϵ is the porosity and τ_m is the appropriate ratio of diffusion coefficients. For a salt–sugar interface, the ratio of buoyancy fluxes is close to $\tau^{\frac{1}{2}}$, where τ is the ratio of diffusion coefficients in the fluid.

The heat flux has also been measured and compared with previous measurements of that through the analogous viscous fluid interface. Although it is found that bending of the interface due to horizontal property variations in each convecting layer causes an increased flow of heat through the two-layer system, the heat flux in the porous medium case does not reach the 'solid plane' value. It is inertial fluid motions which

allow this value to be exceeded in the unconstrained fluid. In both cases the heat flux at larger density ratios ($R_\rho = \beta\Delta S/\alpha\Delta T > 3$) can be predicted by considering the interface edge to be a rigid, conducting boundary and assuming that the stabilizing property is only important within the interface. The porosity and the thermal conductivity are important properties of the solid medium: the ratio of salt to heat buoyancy fluxes is proportional to the porosity and the flux of heat through the interface is determined by thermal diffusion through the saturated medium.

An application of these results to a simple two-layer model of the Wairakei geothermal system predicts a ratio of salt and heat fluxes which is consistent with the estimated real value. The postulated presence of a 'diffusive' thermohaline interface is also able to explain other characteristics of the groundwater convection system.

This work was carried out at the Research School of Earth Sciences, The Australian National University. I thank Professor J. S. Turner and Dr A. McNabb for helpful discussions.

REFERENCES

BOOKER, J. R. & HARTLINE, B. K. 1981 A boundary-layer model for thermal convection in a porous medium. Submitted to *J. Fluid Mech.*

CALTAGIRONE, J. P., CLOUPEAU, M. & COMBARNOUS, M. A. 1971 Convection naturelle fluctuante dans une couche poreuse horizontale. *C. R. Acad. Sci. Paris* B **273**, 833–836.

COMBARNOUS, M. & LEFUR, B. 1969 Transfert de chaleur par convection naturelle dans une couche poreuse horizontale. *C. R. Acad. Sci., Paris* B **269**, 1009–1012.

CRAPPER, P. F. 1975 Measurements across a diffusive interface. *Deep-Sea Res.* **22**, 537–545.

DE WIEST, R. J. M. 1969 *Flow Through Porous Media*, pp. 180–181. Academic.

ELDER, J. W. 1967 Steady free convection in a porous medium heated from below. *J. Fluid Mech.* **27**, 29–48.

ELDER, J. W. 1968 The unstable thermal interface. *J. Fluid Mech.* **32**, 69–96.

FOSTER, T. D. 1971 Intermittent convection. *Geophys. Fluid Dyn.* **2**, 201–217.

GRIFFITHS, R. W. 1979 The transport of multiple components through a thermohaline diffusive interface. *Deep-Sea Res.* **26**, 383–397.

GRIFFITHS, R. W. & RUDDICK, B. R. 1980 Accurate fluxes across a salt–sugar finger interface deduced from direct density measurements. *J. Fluid Mech.* **99**, 85–95.

HUPPERT, H. E. 1971 On the stability of a series of double-diffusive layers. *Deep-Sea Res.* **18**, 1005–1021.

LINDEN, P. F. 1974 A note on the transport across a diffusive interface. *Deep-Sea Res.* **21**, 283–287.

LINDEN, P. F. & SHIRTCLIFFE, T. G. L. 1978 The diffusive interface in double-diffusive convection. *J. Fluid Mech.* **87**, 417–432.

MCNABB, A. 1975 Geothermal physics. *Appl. Math. Div. DSIR, New Zealand. Tech. Rep.* no. 32.

MCNABB, A., GRANT, M. A. & ROBINSON, J. L. 1975 *Appl. Math. Div. DSIR, New Zealand. Tech. Rep.* no. 34.

MARMORINO, G. O. & CALDWELL, D. R. 1976 Heat and salt transport through a diffusive thermohaline interface. *Deep-Sea Res.* **23**, 69–67.

NIELD, D. A. 1968 Onset of thermohaline convection in a porous medium. *Water Resources Res.* **4**, 553–560.

ROBINSON, J. L. 1976 Theoretical analysis of convective instability of a growing horizontal thermal boundary layer. *Phys. Fluids* **19**, 778–791.

ROBINSON, J. L. & O'SULLIVAN, M. J. 1976 A boundary-layer model of flow in a porous medium at high Rayleigh number. *J. Fluid Mech.* **75**, 459–467.

RUDDICK, B. R. & SHIRTCLIFFE, T. G. L. 1979 Data for double diffusers: Physical properties of aqueous salt–sugar solutions. *Deep-Sea Res.* A **26**, 775–787.

SAFFMAN, P. G. 1960 Dispersion due to molecular diffusion and macroscopic mixing in flow through a network of capillaries. *J. Fluid Mech.* **7**, 194–208.

SCHMITT, R. W. 1979 Flux measurements on salt fingers at an interface. *J. Mar. Res.* **37**, 419–436.

SHIRTCLIFFE, T. G. L. 1973 Transport and profile measurements of the diffusive interface in double diffusive convection with similar diffusivities. *J. Fluid Mech.* **57**, 27–43.

TURNER, J. S. 1965 The coupled turbulent transports of salt and heat across a sharp density interface. *Int. J. Heat Mass Transfer* **8**, 759–767.

TURNER, J. S. 1967 Salt fingers across a density interface. *Deep-Sea Res.* **14**, 559–611.

TURNER, J. S. 1973 *Buoyancy Effects in Fluids*, p. 251. Cambridge University Press.

WOODING, R. A. 1957 Steady state free thermal convection of liquid in a saturated permeable medium. *J. Fluid Mech.* **2**, 273–285.

WOODING, R. A. 1960 Instability of a viscous liquid of variable density in a vertical Hele Shaw cell. *J. Fluid Mech.* **7**, 501–515.